Facile preparation of cancer cell membrane vehicle loaded with indocyanine green for effective photothermal therapy of cancer

Ying Sun, Jiang Ni, Yiqing Zhao, Qiufang Gao ✉

Department of Pharmacy, the Affiliated Hospital of Jiangnan University (original area of Wuxi Third People's Hospital), No.585, Xingyuan Road (North), Liang Xi District, Wuxi City, Jiangsu Province, People's Republic of China
✉ *E-mail: gqf0526@163.com*

Published in Micro & Nano Letters; Received on 30th March 2020; Revised on 26th May 2020; Accepted on 30th June 2020

In this study, using the lung cancer cells (A549) as the model cell line, the authors proposed a facile method to prepare uniform-sized cancer cell membrane (Ccm) vehicle, which was then employed to load the photothermal agent indocyanine green (ICG) for effective cancer photothermal therapy (PTT). The as-prepared Ccm/ICG was demonstrated to have a uniform particle size of around 100 nm, which was capable of targeting the A549 cells through Ccm-mediated endocytosis. As a result, the Ccm/ICG increased the cellular uptake of Ce6 into A549 cells as compared to free ICG and potentiated the PTT efficacy both in vitro and in vivo, which might be a promising drug delivery system for advanced cancer therapy.

1. Introduction: Lung cancer is one of the most widely observed neoplasm in males and responsible for 29% of the total mortality in tumours around the world [1]. The incidence and mortality of lung cancer are increasing rapidly and it severely endangers human health and life [2]. The development of drug delivery systems (DDSs) suitable for cancer therapy, including lung cancer, is one of the hot research studies in nanomedicine [3–5]. Previous studies have employed materials ranging from naturally occurred ones to artificial kinds to construct DDSs for cancer therapy and showed some promising results [6–8]. However, inevitable shortages including high expense, uncontrollable side effects as well as low reproducibility severely limited the further applications of artificial materials in cancer therapy [9]. As a result, it was generally recognised that naturally occurred materials are more suitable to build DDSs in cancer treatment that chitosan and phospholipids are widely adopted and studied by many previous research studies.

In recent years, the introduction of cell-based vehicle to serve as the DDS has raised the attention of many researchers. Especially, the cell membrane-derived DDS is demonstrated to inherit some of the characteristics of the mother cells including high biocompatibility and homologous recognition [10, 11]. In particular, the cancer cell membrane (Ccm)-based DDS was shown to specifically target the isogenous cancer cells both in vitro and in vivo without significant side effects [12, 13]. As a result, the development of Ccm-based DDS is becoming one of the most convenient and efficient ways to solve the targeting delivery matter in cancer therapy [14, 15]. However, the Ccm application is also limited by several technical restrictions, among which the facile and repeatable large-scale production of the Ccm vehicle is the most difficult case. Herein our study, we introduced a facile method to afford large-scale preparation of uniform and well-dispersed Ccm carrier for potential application as DDS to deliver various drugs for effective cancer therapy. Most importantly, this method can be applicable regardless of cell type upon minor revision based on the adopted cells, which is beneficial to be employed in more extensive applications. The mixture of different cell lines to prepare hybrid Ccm using this protocol also extends the medical applications of this platform.

Photothermal therapy (PTT) is now well recognised as one of the most powerful ways to treat tumour [16]. It kills tumour cells through the thermal conversion capability of the photothermal agent upon laser irradiation. Many previous studies have revealed the significantly enhanced tumour ablation results in PTT as compared to conventional chemotherapy [17, 18]. One of the difficulties that limit further PTT application in cancer therapy is the lack of suitable DDS for precise and effective tumoural delivery of photothermal agents [16]. As far as our concern, the Ccm might be a suitable carrier for the delivery of the photothermal agent for better PTT of cancer due to its well-recognised merits as mentioned above.

Here, in our study, using the lung cancer cells (A549) as the model cell line, we firstly developed a facile method for the large-scale production of Ccm. Afterwards, the model photothermal agent indocyanine green (ICG) was loaded into the as-prepared Ccm to construct a biocompatible and tumour-targeted DDS (Ccm/ICG) for cancer therapy.

2. Materials and method

2.1. Chemicals, cell line, and animal model: The chemicals adopted in our research were from Sigma (MO, USA) unless otherwise stated. The human lung carcinoma cell line (A549) was purchased from ATCC (Virginia, USA) and cultured in Dulbecco's modified eagle medium (Gibco, California, USA) supplied with 10% foetal bovine serum (Gibco, California, USA) under standard conditions as previously reported [19]. Male Balb/c nude mice were purchased from the Model Animal Research Center of Nanjing University (Nanjing, China) and raised in standard specific pathogen free (SPF) condition with sufficient food supply. The A549 tumour-bearing mice were established according to a previous report [20]. All procedures involved in animal studies were approved and supervised by the Animal Ethics Committee of Jiangnan University.

2.2. Preparation of Ccm vehicle and drug loading (Dl) of ICG: The A549 cells at the logarithmic phase were collected and rinsed three times using phosphate-buffered saline (PBS; pH 7.4, 4°C). Afterwards, the cells were incubated with 5 ml PBS (10^7 cells/ml) containing 25 mM paraformaldehyde (PFA) and 2 mM dithiothreitol (DTT) at 37°C for 2 h with gentle agitation (100 rpm, RET basic, IKA, Staufen, Germany). The solution was then centrifuged at 500 g for 10 min (LE-80K, Beckman Coulter, Miami, USA) to remove the cell debris and large aggregates. The supernatant was then subjected to probe sonication (600 W for 30 min, work 2 s and rest 3 s, SM-3000A, Shunma Tech, Nanjing, China) at 4°C. The solution was finally concentrated using centrifugal filter (30 kDa, Millipore, CA, USA) at 5000 g for 0.5 h (LE-80K,

doi: 10.1049/mnl.2020.0208

Beckman Coulter, Miami, USA). The collected solution containing the Ccm was quantified using the BCA kit (Thermo-Fisher, California, USA) according to the manufacturer's instructions and stored at 4°C until further usage.

For the loading of ICG, 200 µl ICG solution (1 mg/ml) was dropwise added into 1 ml of Ccm solution (100 µg/ml protein) under agitation. Afterwards, the solution was allowed to stand at room temperature for 30 min and then subjected to dialysis (10 kDa, 1 l × 5). The collected solution within the dialysis bag was Ccm/ICG.

The Dl in the Ccm/ICG was determined using ultraviolet spectroscopy at 784 nm (UV5Nano, METTLER TOLEDO, Zurich, Switzerland).

2.3. Characterisation: The particle size of the nanoparticles was assessed using Size Analyzer (Omni 90Plus PALS, Brookhaven Instruments, NewYork, USA). The photothermal conversion capability of nanoparticles was performed using previously reported method [21]. The stability and haemolysis of nanoparticles were determined according to a previous report [22].

2.4. Cellular uptake and cell viability: The cellular uptake and cell viability assays were conducted using previously reported protocols [23]. In brief, 1×10^4 A549 cells were seeded on a 24-well plate overnight and then incubated with different formulations at designated drug concentrations with or without laser irradiation.

2.5. In vivo anticancer study: The in vivo anticancer study was performed according to a previous report [24]. In brief, 2×10^6 A549 cells were injected to the flank of mice (4–5 weeks, 20 g). The mice with tumour volume at around 200 mm^3 were used in experiments.

2.6. Statistical analysis: Statistical significance was tested by two-tailed Student's *t*-test or one-way analysis of variance with $^*P<0.05$ as statistically significant.

3. Results and discussion

3.1. Preparation of Ccm vehicle and photothermal conversion capability of Ccm/ICG: The Ccm was firstly produced using a facile sulphydryl blocking method. In brief, the DTT was introduced to break the disulphide bonds of the cell to finally result in cell dissociation. By carefully adjusting the DTT concentration, cell density as well as the incubation temperature and time, the size of most of the resulted Ccm can be controlled to a specific size range. After separation of the large aggregates (including organelles and impurities), the obtained supernatant was then subjected to gentle probe sonication to allow the homogenisation of Ccm. Afterwards, the Ccm was concentrated using a centrifugal filter for further usage [25]. As shown in Fig. 1*a*, under the given preparation condition, the obtained Ccm was well-dispersed nanoparticles with average size distribution at around 100 nm. It was well recognised that nanoparticles with a size around 100 nm can most preferably take advantage of the enhanced penetration and retention effect of the tumour tissue for better accumulation in tumour tissue. We speculated that Ccm might be a suitable vehicle for tumour-targeted delivery of drugs with the combination of passive and positive targeting strategies. The ICG was then loaded into Ccm through the hydrophobic interaction between the ICG molecule and the phospholipid bilayer of Ccm. The ICG was then encapsulated in the bilayer to hide from the hostile environments upon in vivo applications. As shown in the inserted image of Fig. 1*a*, the TEM image showed that the Ccm/ICG was spheroid nanoparticles with size at around 100 nm, which was similar to that of Ccm, suggesting that the Dl of ICG did not significantly affect the size and morphology of Ccm, which was in line with previous reports [26].

The ICG as an amphipathic molecule was capable of harbouring in the hydrophobic region of the lipid bilayers. As a result, the Ccm

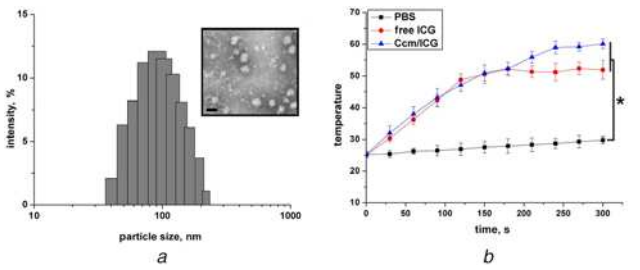

Fig. 1 *Size and photothermal profile of Ccm/ICG*
a Size distribution of Ccm
b Photothermal conversion capability of Ccm/ICG. The aqueous solution of free ICG and Ccm/ICG (2 mL, ICG concentration: 5 mg/ml) was subjected to 808 nm irradiation (1 W/cm^2) for 5 min. Inserted image is the TEM image of Ccm/ICG. Scale bar: 100 nm. The experiments were repeated thrice in a parallel manner and the results were expressed as mean value and standard deviation ($n = 3$). $^*P<0.05$

can provide favourable protection to the ICG to avoid the premature excretion upon in vivo applications. In particular, the photothermal conversion capability of ICG was the most important parameter to be evaluated. Therefore, the comparative photothermal conversion of free ICG and Ccm/ICG was investigated. As shown in Fig. 1*b*, laser irradiation without photothermal agent resulted in only a minor increase in temperature. In contrast, the free ICG showed significant elevation on solution temperature upon laser irradiation. It was noted that the temperature in the free ICG group suffered a slight drawback after 150 s, which might be due to the accelerated degradation of ICG in high temperature, suggesting its instability in aqueous solution and was in line with the previous report [27]. However, the temperature in Ccm/ICG group consistently grows to over 60°C without drawbacks at the high temperature, indicating the preferable protection of Ccm on ICG might alleviate the degradation of ICG to maintain photothermal conversion for better PTT of cancer.

3.2. Stability and biocompatibility of Ccm/ICG: To determine the stability and biocompatibility of Ccm/ICG to be a DDS for cancer therapy. The size changes of Ccm/ICG in both PBS and mouse plasma were monitored to reveal the stability profile of Ccm/ICG in physiological environments. As displayed in Fig. 2*a*, it was observed that the size of Ccm/ICG remained largely unchanged for 48 h in both media, which suggested that Ccm/ICG can remain stable under physiological environments upon in vivo applications. This is beneficial for Ccm/ICG to precisely deliver loaded cargo to the tumour tissue as it was generally recognised that the change in particles usually indicates the deformation of

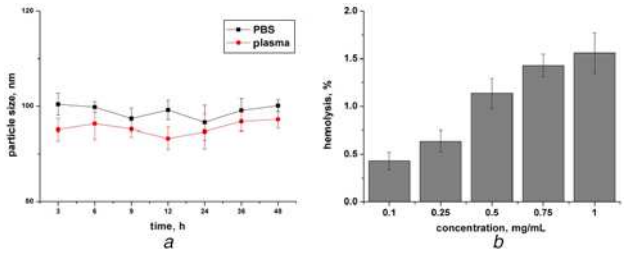

Fig. 2 *Biocompatibility of Ccm/ICG*
a Stability of Ccm/ICG in PBS (0.01 M, PBS) and mouse plasma at the nanoparticle concentration of 0.5 mg/ml for 48 h
b Haemolysis of Ccm/ICG on 2% RBC of the mouse at different nanoparticle concentrations. RBCs suspension incubated with saline and distilled water under the same condition were employed as negative (0% haemolysis) and positive controls (100% haemolysis), respectively. The experiments were repeated thrice in the parallel manner and the results were expressed as mean value and standard deviation ($n = 3$)

DDS and the leakage of drugs. In addition, it was also suggested that the Ccm prepared in our study under a given condition was a highly reproducible vehicle, which might be adopted in the application of other biomedical fields.

The haemolysis as another parameter to be considered in drug delivery was also studied using red blood cells (RBCs) of a mouse. After incubation with Ccm/ICG, the leakage of haemoglobin was measured (indicating the damage of RBC structure). As illustrated in Fig. 2*b*, although the haemolysis ratio of Ccm/ICG increased as a function of DDS concentration, the haemolysis rate at the highest DDS concentration (1 mg/ml) was no more than 2%, which was considered as low haemolysis risk as it was much lower under the 5% threshold. Moreover, according to a previous report [28], due to the dilution of the circulation system, the general DDS concentration in the body would be much lower than 1 mg/ml. Therefore, the Ccm/ICG can be recognised as a highly biocompatible DDS for cancer therapy.

3.3. Cellular uptake and cell viability: The cellular uptake of Ccm/ICG in A549 cells was studied and incubation of the cells with the DDS for different time intervals with or without pre-treatment of CCM. As shown in Fig. 3*a*, free ICG showed inferior uptake in A549 cells, which might be due to its amphipathicity nature. Since the cells were surrounded by the lipid bilayer, it was suggested that hydrophobic molecules or materials with a similar structure or nature are more preferably taken up by cells. As proof of concept, the cellular uptake of Ccm/ICG under the same conditions was also evaluated. As expected, the Ccm/ICG showed much more enhanced intracellular accumulation than free ICG and this tendency further increased as time extended. Based on these results, it was concluded that Ccm/ICG can increase the delivery of ICG molecules into the A549 cells, which might provide better PTT outcomes in the anticancer studies.

To further confirm the positive role of Ccm in the increased cellular uptake of Ccm/ICG in A549 cells. The cellular uptake was commenced after cells were pre-treated with Ccm (20 μg/ml of protein) for 1 h. interestingly, the cellular uptake of ICG with or without Ccm pre-treatment showed almost unaffected. In contrast, the cellular uptake of Ccm/ICG was significantly varied. In detail, the intracellular signal was dropped to only 66.4% of the original level at 6 h post incubation, suggesting the critical roles of Ccm in the endocytosis of Ccm/ICG. According to the previous report [29], it was suggested that the binding proteins expressed on the surface of Ccm were also inherited to the Ccm vehicle after preparation in DDS. As a result, the binding proteins can specifically recognise the isogenous cells to afford recognition and the following uptake, which was beneficial to potentiate the drug accumulation in target cells.

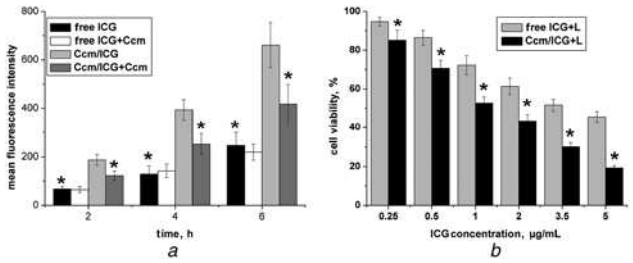

Fig. 3 *Uptake and in vitro anticancer profile of Ccm/ICG*
a Quantitative analysis of intracellular time-dependent uptake of different formulations in A549 cells (pretreated with/without excess Ccm for 1 h) using flow cytometry. **P*<0.05 versus Ccm/ICG
b Viability of A549 cells treated with different formulations at different ICG concentrations for 48 h. The cells were subjected to 808 nm irradiation (1 W/cm^2) for 5 min. **P*<0.05 versus free ICG. The experiments were repeated thrice in the parallel manner and the results were expressed as mean value and standard deviation (n = 3)

To study the in vitro anticancer benefits resulting from the enhanced cellular uptake, the cell viability of A549 cells after PTT of different formulations was evaluated. As shown in Fig. 3*b*, it was clearly observed that PTT could exert significantly killing effects on A549 cells upon 808 nm laser irradiation. Moreover, the Ccm/ICG could achieve much more elevated benefits than free ICG under the same condition. It was noted that this effect was further increased as a function of drug concentration. It was suggested that the enhanced cell killing effect of Ccm/ICG as compared to free ICG might come from two aspects: (i) the Ccm offers well protection to the encapsulated ICG molecules in aqueous condition without the loss of its photothermal conversion nature, which facilitate the continuous photothermal conversion of Ccm/ICG in cells. (ii) The enhanced cellular uptake of Ccm/ICG due to the Ccm-mediated endocytosis further enhanced the intracellular concentrations of ICG, which might resulted in a more higher intracellular temperature for be头疼人cell killing upon laser irradiation.

3.4. In vivo anticancer study: Based on the exciting results in cellular assays, we then study the in vivo assay to further verify the beneficial effects of Ccm/ICG in PTT of lung cancer. The A549 oxengrafted Balb/c nude mice model was established and recruited for study when the tumour volume reached 200 mm^3. As shown in Fig. 4*a*, in line with the previous report [30], the saline group without any treatment showed rapid and consistent growth in tumour volume, which exceeded 100 mm^3 at the end of the test. The intervene of PTT using free ICG showed some advances in tumour ablation, which significantly retarded the growth of tumour volume during the whole study. Most importantly, the introduction of Ccm/ICG achieved the most powerful tumour ablation which reverses the growth of tumours to a small volume of 52 ± 15 mm^3 at the end of the test. The haematoxylin and eosin (HE) staining was further performed on the excised tumours from each group. As depicted in Fig. 4*b*, the tumour sections from the saline group showed high cell viability and cell confluence which indicated the severe progression of cancer cells. The treatment of PTT using fresh ICG showed decreased cell viability as well as cell confluence, which was in line with results in Fig. 4*a*. As expected, the treatment using Ccm/ICG resulted in structure damage (shown as a white cavity in the tumour section) which might be due to the thermal ablation of PTT. Consistently, the

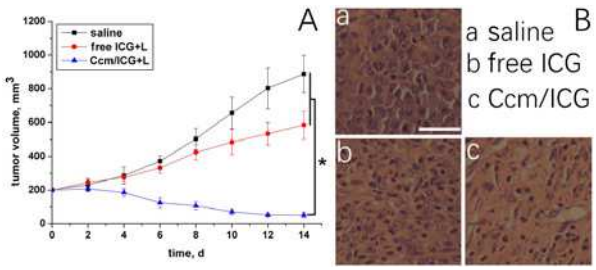

Fig. 4 *In vivo anticancer profile of Ccm/ICG*
a Tumour volume variations of A549 oxengrafted Balb/c nude mice being treated with different formulations. Eighteen A549 tumour-bearing mice were divided randomly into three groups and intravenously administered with different formulations for seven times in 14 days. The given ICG was 5 mg/kg and all mice were subjected to laser irradiation of 0.5 W/cm^2 (5 min) after 24 h post-administration. During the test, variations in tumour volume were monitored before every administration. The experiments were repeated thrice in the parallel manner and the results were expressed as mean value and standard deviation (n = 6). **P*<0.05
b HE staining of tumour tissues from each group at the end of the assay. After the final day of collecting measurements, three mice from each group were randomly selected and sacrificed, and their tumour tissues were extracted and subjected to HIM staining. Scale bar: 100 μm

doi: 10.1049/mnl.2020.0208

cell viability as well as cell confluence was also significantly reduced as compared to the other groups.

These significantly increased benefits were much more powerful than those acquired in cellular studies, which might due to the precise and effective in vivo ICG delivery using Ccm. According to the previous report [31], the in vivo administration of ICG usually suffered from quick elimination and excretion due to the amphipathicity of ICG. Moreover, the aqueous instability of ICG further diminishes the total accumulation of valid drug concentration in tumours. In contrast, the Ccm/ICG resolved all the above-mentioned problems to offer enhanced stability, precise targetability as well as elevated intracellular accumulation, which finally resulted in a nearly full ablation of tumours.

4. Conclusion: In our study, we report a facile method to prepare Ccm with well-dispersed size range at 100 nm using A549 cells as the model cell line. The ICG-loaded Ccm (Ccm/ICG) was able to serve as a highly biocompatible with specific tumour targetability for the PTT of lung cancer. The Ccm/ICG is not only able to preserve the photothermal conversion capability of ICG but also capable of alleviating the aqueous instability of ICG upon laser irradiation. Most importantly, the Ccm/ICG could realise much more enhanced cellular accumulation of ICG in A549 cells as compared to free ICG. The enhanced stability, precise targetability, as well as elevated intracellular accumulation of Ccm/ICG, achieved potent anticancer effects on A549 cells in vitro with a nearly full ablation of tumours in vivo.

5 References

[1] Li Z., Wu H., Yang M., *ET AL.*: 'Stability mechanism of O/W pickering emulsions stabilized with regenerated cellulose', *Carbohydr. Polym.*, 2018, **181**, pp. 224–233

[2] Mok T.S., Wu Y.-L., Ahn M.-J., *ET AL.*: 'Osimertinib or platinum-pemetrexed in EGFR T790M-positive lung cancer', *N. Engl. J. Med.*, 2017, **376**, (7), pp. 629–640

[3] Kumar S.U., Kumar V., Priyadarshi R., *ET AL.*: 'pH-responsive prodrug nanoparticles based on xylan-curcumin conjugate for the efficient delivery of curcumin in cancer therapy', *Carbohydr. Polym.*, 2018, **188**, pp. 252–259

[4] Jahanban-Esfahlan R., de la Guardia M., Ahmadi D., *ET AL.*: 'Modulating tumor hypoxia by nanomedicine for effective cancer therapy', *J. Cell. Physiol.*, 2018, **233**, (3), pp. 2019–2031

[5] Cao L., Zhang H., Zhou Z., *ET AL.*: 'Fluorophore-free luminescent double-shelled hollow mesoporous silica nanoparticles as pesticide delivery vehicles', *Nanoscale*, 2018, **10**, (43), pp. 20354–20365

[6] Zhang S., Pang G., Chen C., *ET AL.*: 'Effective cancer immunotherapy by ganoderma lucidum polysaccharide-gold nanocomposites through dendritic cell activation and memory T cell response', *Carbohydr. Polym.*, 2019, **205**, pp. 192–202

[7] Zhao X., Tang D., Wu Y., *ET AL.*: 'An artificial cell system for biocompatible gene delivery in cancer therapy', *Nanoscale*, 2020, **12**, (18), pp. 10189–10195

[8] Li L., Yang S., Song L., *ET AL.*: 'An endogenous vaccine based on fluorophores and multivalent immunoadjuvants regulates tumor micro-environment for synergistic photothermal and immunotherapy', *Theranostics*, 2018, **8**, (3), p. 860

[9] Liu L.H., Qiu W.X., Zhang Y.H., *ET AL.*: 'A charge reversible self-delivery chimeric peptide with cell membrane-targeting properties for enhanced photodynamic therapy', *Adv. Funct. Mater.*, 2017, **27**, (25), p. 1700220

[10] Chen Z., Zhao P., Luo Z., *ET AL.*: 'Cancer cell membrane-biomimetic nanoparticles for homologous-targeting dual-modal imaging and photothermal therapy', *ACS Nano*, 2016, **10**, (11), pp. 10049–10057

[11] Fang R.H., Hu C.M., Luk B.T., *ET AL.*: 'Cancer cell membrane-coated nanoparticles for anticancer vaccination and drug delivery', *Nano Lett.*, 2014, **14**, (4), pp. 2181–2188

[12] Byun D.J., Wolchok J.D., Rosenberg L.M., *ET AL.*: 'Cancer immunotherapy – immune checkpoint blockade and associated endocrinopathies', *Nat. Rev. Endocrinol.*, 2017, **13**, (4), p. 195

[13] Nie D., Dai Z., Li J., *ET AL.*: 'Cancer-cell-membrane-coated nanoparticles with a yolk–shell structure augment cancer chemotherapy', *Nano Lett.*, 2019, **20**, (2), pp. 936–946

[14] Golchin S., Alimohammadi R., Rostami Nejad M., *ET AL.*: 'Synergistic antitumor effect of anti-PD-L1 combined with oxaliplatin on a mouse tumor model', *J. Cell. Physiol.*, 2019, **234**, (11), pp. 19866–19874

[15] Zhu Y., Yu F., Tan Y., *ET AL.*: 'Reversing activity of cancer associated fibroblast for staged glycolipid micelles against internal breast tumor cells', *Theranostics*, 2019, **9**, (23), pp. 6764–6779

[16] Peng J., Xiao Y., Li W., *ET AL.*: 'Photosensitizer micelles together with IDO inhibitor enhance cancer photothermal therapy and immunotherapy', *Adv. Sci.*, 2018, **5**, (5), p. 1700891

[17] Zhao M., Xu Y., Xie M., *ET AL.*: 'Halogenated aza-BODIPY for imaging-guided synergistic photodynamic and photothermal tumor therapy', *Adv. Healthcare Mater.*, 2018, **7**, (18), p. 1800606

[18] Xu G., Bao X., Chen J., *ET AL.*: 'In vivo tumor photoacoustic imaging and photothermal therapy based on supra-(carbon nanodots)', *Adv. Healthcare Mater.*, 2019, **8**, (2), p. 1800995

[19] Duan M., Xia F., Li T., *ET AL.*: 'Matrix metalloproteinase-2-targeted superparamagnetic Fe_3O_4-PEG-G5-MMP2@Ce6 nanoprobes for dual-mode imaging and photodynamic therapy', *Nanoscale*, 2019, **11**, (39), pp. 18426–18435

[20] Wang C., Han M., Liu X., *ET AL.*: 'Mitoxantrone-preloaded water-responsive phospholipid-amorphous calcium carbonate hybrid nanoparticles for targeted and effective cancer therapy', *Int. J. Nanomed.*, 2019, **14**, pp. 1503–1517

[21] Pan H., Sun Y., Cao D., *ET AL.*: 'Low-density lipoprotein decorated and indocyanine green loaded silica nanoparticles for tumor-targeted photothermal therapy of breast cancer', *Pharm. Dev. Technol.*, 2020, **25**, (3), pp. 308–315

[22] Tang D., Zhao X., Yang T., *ET AL.*: 'Paclitaxel prodrug based mixed micelles for tumor-targeted chemotherapy', *RSC Adv.*, 2018, **8**, (1), pp. 380–389

[23] Yang D., Yang G., Sun Q., *ET AL.*: 'Carbon-dot-decorated TiO_2 nanotubes toward photodynamic therapy based on water-splitting mechanism', *Adv. Healthc. Mater.*, 2018, **7**, (10), p. 1800042

[24] Liu X., Wang C., Ma H., *ET AL.*: 'Water-responsive hybrid nanoparticles codelivering ICG and DOX effectively treat breast cancer via hyperthermia-aided DOX functionality and drug penetration', *Adv. Healthc. Mater.*, 2019, **8**, (8), p. 1801486

[25] Ingato D., Edson J.A., Zakharian M., *ET AL.*: 'Cancer cell-derived, drug-loaded nanovesicles induced by sulfhydryl-blocking for effective and safe cancer therapy', *ACS Nano*, 2018, **12**, (9), pp. 9568–9577

[26] Zhang J., Miao Y., Ni W., *ET AL.*: 'Cancer cell membrane coated silica nanoparticles loaded with ICG for tumour specific photothermal therapy of osteosarcoma', *Artif. Cells Nanomed. Biotechnol.*, 2019, **47**, (1), pp. 2298–2305

[27] Tang Y., Li Y., Li S., *ET AL.*: 'Transformable nanotherapeutics enabled by ICG: towards enhanced tumor penetration under NIR light irradiation', *Nanoscale*, 2019, **11**, (13), pp. 6217–6227

[28] Egloff-Juras C., Bezdetnaya L., Dolivet G., *ET AL.*: 'NIR fluorescence-guided tumor surgery: new strategies for the use of indocyanine green', *Int. J. Nanomed.*, 2019, **14**, p. 7823

[29] Yang J., Teng Y., Fu Y., *ET AL.*: 'Chlorins e6 loaded silica nanoparticles coated with gastric cancer cell membrane for tumor specific photodynamic therapy of gastric cancer', *Int. J. Nanomed.*, 2019, **14**, p. 5061

[30] Zhang Y., Cheng M., Cao J., *ET AL.*: 'Multivalent nanoparticles for personalized theranostics based on tumor receptor distribution behavior', *Nanoscale.*, 2019, **11**, (11), pp. 5005–5013

[31] Xie W., Zhu S., Yang B., *ET AL.*: 'The destruction of laser-induced phase-transition nanoparticles triggered by low-intensity ultrasound: an innovative modality to enhance the immunological treatment of ovarian cancer cells', *Int. J. Nanomed.*, 2019, **14**, p. 9377